Asymmetry of Glia near Central Synapses Favors Presynaptically Directed Glutamate Escape

Knut Petter Lehre*† and Dmitri A. Rusakov*

*Institute of Neurology, University College London, Queen Square, London WC1N 3BG, United Kingdom, and †Department of Anatomy, Institute of Basic Medical Sciences, University of Oslo, N-0317 Oslo, Norway

ABSTRACT Recent findings demonstrate that synaptically released excitatory neurotransmitter glutamate activates receptors outside the immediate synaptic cleft and that the extent of such extrasynaptic actions is regulated by the high affinity glutamate uptake. The bulk of glutamate transporter systems are evenly distributed in the synaptic neuropil, and it is generally assumed that glutamate escaping the cleft affects pre- and postsynaptic receptors to a similar degree. To test whether this is indeed the case, we use quantitative electron microscopy and establish the stochastic pattern of glial occurrence in the three-dimensional (3D) vicinity of two common types of excitatory central synapses, stratum radiatum synapses in hippocampus and parallel fiber synapses in cerebellum. We find that the occurrence of glia postsynaptically is strikingly higher (3–4-fold) than presynaptically, in both types of synapses. To address the functional consequences of this asymmetry, we simulate diffusion and transport of synaptically released glutamate in these two brain areas using a detailed 3D compartmental model of the extracellular space with glutamate transporters arranged unevenly, in accordance with the obtained experimental data. The results predict that glutamate escaping the synaptic cleft is 2–4 times more likely to activate presynaptic compared to postsynaptic receptors. Simulations also show that postsynaptic neuronal transporters (EAAT4 type) at dendritic spines of cerebellar Purkinje cells exaggerate this asymmetry further. Our data suggest that the perisynaptic environment of these common central synapses favors fast presynaptic feedback in the information flow while preserving the specificity of the postsynaptic input.

INTRODUCTION

It has been well documented that glutamate released at common types of hippocampal or cerebellar synapses can activate extrasynaptic receptors. These actions have been shown to increase in the presence of glutamate uptake blockers, indicating a critical role of transporters in restricting the extent of glutamate spillover (Min et al., 1998; Scanziani et al., 1996; Asztely et al., 1997; Carter and Regehr, 2000). Transporters that play a major role in glutamate removal in the brain have been identified (including two main glial transporters, EAAT1–2, also known as GLAST/GLT, and one neuronal type, EAAT4) and characterized (Arriza et al., 1994; Wadiche et al., 1995; Levy et al., 1998; Fairman et al., 1995; Pines et al., 1992; Danbolt, 2001). Glia are thought to carry the bulk of glutamate uptake systems whereas the neuronal EAAT4 transporter is located strategically outside synaptic clefts on dendritic spines of Purkinje cells in the cerebellum (Dehnes et al., 1998; Furuta et al., 1997). It has recently been demonstrated that glial coverage of synapses directly regulates activation of extrasynaptic metabotropic receptors in the hypothalamus (Oliet et al., 2001). The kinetics of glutamate transporters has been established using cell-expression systems and by analyzing the uptake currents in cells or excised membrane patches in brain slices, as summarized in Table 1.

In physiological studies, the extent of glutamate spillover has normally been assumed to affect pre- and postsynaptic receptors (located outside the immediate cleft) to a similar degree. Very recently, however, it has been noted that neuronal glutamate transporters (EAAT4) located outside the synaptic cleft on cerebellar Purkinje cells, inhibit activation of metabotropic glutamate receptors that occur within the same membrane loci (Brasnjo and Otis, 2001). Do glial transporters, which provide the bulk of glutamate uptake, also reduce extracellular glutamate transients at the strategic locations with respect to the release site? At the sub-micron scale, specific immunogold labeling of major glial transporters shows a relatively homogeneous pattern in the glial plasmalemma in the synaptic neuropil (although the labeling is lower wherever glia face cell bodies or blood vessels) (Chaudhry et al., 1995; Furuta et al., 1997; Dehnes et al., 1998; Lehre et al., 1995; Lehre and Danbolt, 1998). What remains unknown, however, is whether the glial membranes that carry these transporters also occur evenly with respect to the synapse and, if they do not, whether this has any significant effect on the extent and preferred direction of glutamate escape.

Direct measurements of fast glutamate transients in the synaptic vicinity have not been possible, and therefore considerable attention has been paid to the predictions of biophysical modeling (Bartol et al., 1991; Uteshev and Pennefather, 1996; Kleinle et al., 1996; Wahl et al., 1996; Clements, 1996; Kruk et al., 1997; Trommershauser et al., 1999). Recently, a compartmental model was described that

Submitted October 21, 2001 and accepted for publication February 17, 2002.

Address reprint requests to: Dmitri Rusakov, Institute of Neurology, University College London, London WC1N 3BG, UK. Tel.: +44-207-837-3611 ext. 4336; Fax: +44-207-278-5616; E-mail: d.rusakov@ion.ucl.ac.uk.

0006-3495/02/07/125/10 $2.00

TABLE 1 Kinetic parameters of identified glutamate transporters: Summary

Transporter	Cell system, preparation	K_m (μM)	k_1 ($M^{-1}s^{-1}$)	k_2, s^{-1} (cycling)	Reference
EAAT1 (GLAST)	*Xenopus* oocytes	20			(Arriza et al., 1994)
	Bergmann glia (patches)	58			(Bergles et al., 1997)
	Astricytes (patches)			~86	(Bergles and Jahr, 1998)
	Xenopus oocytes	12			(Klockner et al., 1994)
	Xenopus oocytes		$>6.8 \times 10^6$		(Wadiche and Kavanaugh, 1998)
EAAT2 (GLT)	Hippocampus		$>10^6$		(Diamond and Jahr, 1997)
	Chinese hamster ovary	17			(Levy et al., 1998)
	Xenopus oocytes	18			(Arriza et al., 1994)
	Kidney 293 cells (patches)	95	1.7×10^6*		(Otis and Kavanaugh, 2000)
	Xenopus oocytes			15	(Wadiche et al., 1995)
EAAT4 (neuronal)	*Xenopus* oocytes	2	1.7×10^6		(Fairman et al., 1995)
	Purkinje cells (patches)	<10		13	(Otis et al., 1997)
	Purkinje cells	≈0		16	(Auger and Attwell, 2000)

*Measured for kainate

reproduces the typical synaptic environment from experimental morphometric data (Rusakov and Kullmann, 1998) including the uneven distribution of glial sheaths (Rusakov, 2001). Although simulations with this model explored the role of perisynaptic glia in extrasynaptic glutamate escape under various conditions of glial coverage (Rusakov, 2001), the actual pattern of glial occurrence near the synapses of interest remained unknown.

In the present study, therefore, we use quantitative electron microscopy and apply methods of mathematical morphology to establish the distribution of glia and glial membranes near stratum radiatum synapses in area CA1 of the hippocampus and parallel fiber (PF) synapses in cerebellum, two common types of central synapses. The data reveal a profound pre- versus postsynaptic asymmetry in the occurrence of glia. To assess the physiological consequences of this asymmetry, we reproduce this synaptic environment in a 3D compartmental model, which incorporates glutamate transporters and diffusion obstacles in strict correspondence with our present and previous experimental observations. Simulating release, diffusion and transport of glutamate with this model predicts that extrasynaptic actions of glutamate near these synapses favor presynaptic, compared to postsynaptic, receptors. This may have important implications in our understanding of how the information flow is processed in the brain.

MATERIALS AND METHODS

Electron microscopy and mathematical morphology

Ultrathin (60–90 nm) serial sections of hippocampal area CA1 and the molecular layer of cerebellum were prepared from 7–8-week-old male rats, and the ultrastructural tissue components were identified from stacks of adjacent sections as described in detail earlier (Lehre and Danbolt, 1998), in line with commonly accepted criteria (Ventura and Harris, 1999; Xu-Friedman et al., 2001). Electron micrographs were stored as stacks of digital images and processed using in-house written macros for NIH Image. Major architectural parameters of the neuropil were assessed using image analysis and the laws of exact stereology, as described earlier (Rusakov and Kullmann, 1998; Rusakov et al., 1998). In brief, micrographs of synapses and the surrounding tissue (2-μm-wide planar sections roughly perpendicular to the synaptic cleft) were transformed into the binary outlines of the visible extracellular gaps, as illustrated in Fig. 1, *A* and *B*. Within the micrograph area *A*, we used mathematical morphology routines to compute: the doubled cumulative length of these two-dimensional (2D) outlines, L_A; the cumulative length of the glial membrane profiles, L^*_A; and the cumulative area of glial profiles, S^*_A (Fig. 1 *D*). From these data, the ratio L^*_A/L_A estimated the surface area fraction of glial membranes versus all cell membranes, $4L_A/\pi$ estimated the volume density of the cell surface area, and $4S^*_A/\pi$ estimated the volume fraction of glia in the synaptic vicinity, in accordance with the basics of exact stereology (Underwood, 1970). The level of GLAST/GLT in the extracellular space, C_E, was estimated in our previous study from stereological quantities of glia, quantitative immunoelectron labeling and immunoblot analysis of identified transporters (Lehre and Danbolt, 1998). Because the glial membranes represent the fraction L^*_A/L_A of all cell membranes, the transporter level in the extracellular space adjacent to glia was calculated as $0.5C_EL_A/L^*_A$, which is the lower estimate assuming that glia always face neurons (the upper, less plausible estimate is C_EL_A/L^*_A assuming that glia always face glia). Similarly, the local density of EAAT4 transporters on Purkinje cell dendritic spines was estimated from the formula

$$\frac{0.5C_E \times (4L_A/\pi)}{2\pi R_c^2 \times N_v} \quad (1)$$

where C_E is the average extracellular level of EAAT4 transporters; $2\pi R_c^2$ represents the average extrasynaptic surface area of the typical postsynaptic element (obstacle to diffusion) approximated by a hemisphere adjacent to the synaptic cleft of radius R_c; $N_V = 0.8\ \mu m^{-3}$ is the volume density of synapses in cerebellum (Harvey and Napper, 1988), and $4L_A/\pi$ estimates the cell membrane area per unit tissue volume (see below and Table 2 for parameter values). We made no attempt to correct for the two potential sources of error in these estimates, i.e., local deviations from the uniform transporter density in glial membranes, and that a proportion of the identified transporter proteins could represent nonfunctional transporters. Although the former appears unbiased, the latter is likely to overestimate the transporter density, which will, in turn, underestimate glutamate escape.

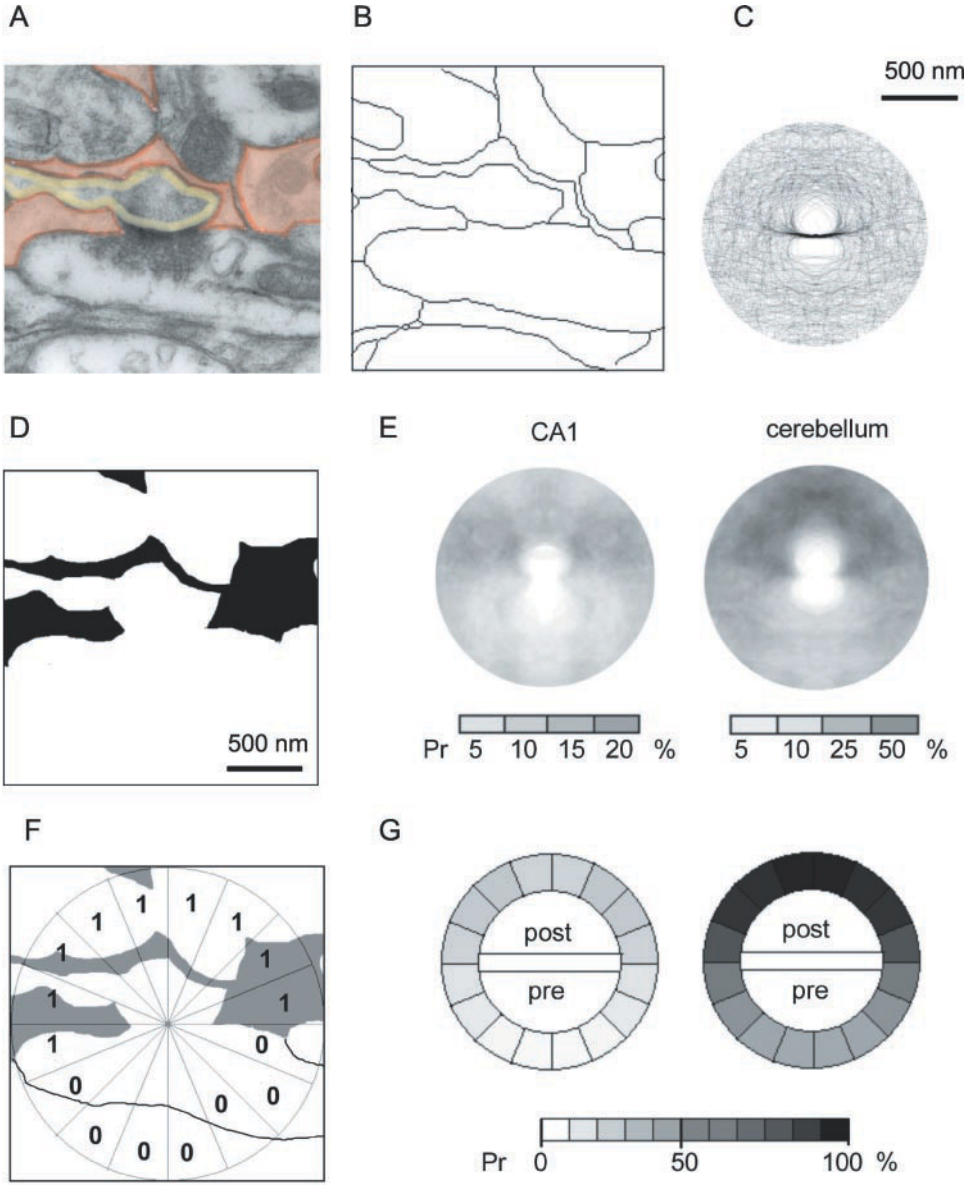

FIGURE 1 Perisynaptic environment and glial coverage at hippocampal and cerebellar synapses. (*A*) A characteristic electron micrograph of the PF synapse in cerebellum; glial profile (*red shading*) was identified using four adjacent sections; postsynaptic structures are outlined in yellow. (*B*) Binary transform of (*A*) where the extracellular space profile is shown by one-pixel lines; their total doubled accumulated length per unit micrograph area represents stereological quantity L_A (see Methods). (*C*) Average of 40 binary-transformed PF synaptic images similar to (*B*), centered and aligned. (*D*) Binary transform of (*A*) where glial profiles are filled with black pixels; their total accumulated area per unit micrograph area represents quantity S^*_A and their total outline perimeter represents L^*_A (see Methods). (*E*) Stack average of images similar to (*D*) representing 80 area CA1 (*left*) and 40 PF synapses (*right*); gray levels are proportional to the occurrence of glia. (*F*) Binary image in (*D*) superimposed with an azimuth grid: digits show whether the perisynaptic membrane (membrane profile that could be traced to the synaptic cleft) is adjacent (>50% contact) to glia within the sector; presynaptic terminal is outlined. (*G*) Diagrams showing the probability (*gray scale*) of a direct contact between glia and the perisynaptic membrane in area CA1 (*left*) and near PF synapses (*right*); the values represent average scores, as shown in (*F*). *Pr*, probability scale bar; scale bars in (*C*) and (*D*) apply throughout except in (*G*).

The probabilistic pattern of the occurrence of glia and glial membranes in the synaptic vicinity was determined by analyzing the stacks of binary-transformed, rotated and aligned synaptic images, as described in the Results.

Perisynaptic environment: compartmental model

The 3D compartmental model used was described in detail earlier (Rusakov, 2001). As suggested by the characteristic occurrence of the extracellular space around the area CA1 synapses (Rusakov and Kullmann, 1998) and PF synapses (see Results below), the perisynaptic environment can be approximated by two hemispheres (which represent the typical, pre- and postsynaptic, obstacles to diffusion), the synaptic apposition zone, and the surrounding porous neuropil (tortuosity $\lambda \sim 1.4$) separated from the hemispheres by a 25-nm extracellular gap. The extracellular space fraction in area CA1, $\alpha = 0.12$, was estimated from electron micrographs in our previous work (Rusakov and Kullmann, 1998), and was in line with the estimate of $\alpha = 0.14$ assessed from diffusion measurements in hippocam-

TABLE 2 Major stereological quantities for glia and glutamate transporters

Parameter	CA1	cerebellum
Glia volume fraction, %	9.71 ± 0.83	32.6 ± 2.6
ECS fraction, α	0.12*	0.11
Total cell surface area density $\mu m^2/\mu m^3$	14.1 ± 0.22*	12.3 ± 0.33
	14†	14†
Glia surface area, $\mu m^2/\mu m^3$	1.78 ± 0.10	4.82 ± 0.24 (39%)
(fraction of total)	1.4†	3.8 (27%)†
GLAST/GLT, tissue-average, mM	0.2†	0.25†
GLAST/GLT, near glia, mM	1.0†	0.5†
EAAT4, tissue-average, mM	Low	0.029†
EAAT4, near postsynaptic elements, mM	Low	0.9‡

Transporter levels are given as the effective concentrations in the extracellular space.
*Data from (Rusakov and Kullmann, 1998).
†Data from (Lehre and Danbolt, 1998).
‡Calculated from the average EAAT4 levels, numeric density of PF synapses and the average size of PF elements, as explained in Methods.
Other parameters were estimated in the present study.

pal slices (Perez-Pinon et al., 1995) (however, see Mazel et al., 1998). The space in the model was partitioned in the radial (step $\delta R = 25$ nm) and the tangential (angular step $\pi/9$) directions. The glutamate concentration within each compartment at each time step was computed using the mass transfer balance, and the flux between adjacent compartments was computed using the Fick's first law, exactly as described previously (Rusakov, 2001). In total, 2000–3000 compartments comprised the synaptic environment, and the glutamate level was clamped at zero at 5 μm. The compliance with the law of mass conservation (including free, bound, and taken up glutamate) was tested at each time step, as described previously (Rusakov, 2001).

The average synaptic size R_c was 0.22 μm for CA1 synapses and 0.41 μm for PF synapses, in accordance with morphological observations. The extracellular diffusion coefficient for glutamate was initially set at 0.3 μm^2/ms, and then varied within the physiological limits to explore the consequences. $N = 5000$ molecules of glutamate were released into the synaptic cleft center with an α-function rate $\sigma^2 te^{-\sigma t}$ where $\sigma = 39$ ms^{-1} (Stiles et al., 1996). Outside the immediate synapse, the free-to-porous transition was accounted for by scaling the outward flux (diffusion source strength) and D with factors $1/\alpha$ and $1/\lambda^2$, respectively, at the porous medium boundary. The residual binding to main ionotropic glutamate receptors (AMPA and NMDA types) was set to match their estimated average level of 10 μM ($K_d = 20$ μM), as discussed earlier (Rusakov, 2001).

Glutamate transport in the synaptic vicinity

The levels of GLT/GLAST in space compartments adjacent to the synaptic structure were set proportional to the measured average occurrence of glial membranes (see Fig. 1 *G* and Results below) and normalized against their average near-glia extracellular level (Table 2). This pattern was also held in more distal compartments to match the occurrence of glia in space (Fig. 1 *E*). Outside the perisynaptic region where the asymmetry of glial distribution occurred (0.8–1.0 μm from the center, see Fig. 1 *E*), the transporters were distributed evenly at their average extracellular level (see Table 2). At the cerebellar Purkinje cell synapses, transporters EAAT4 were arranged on the postsynaptic hemisphere surface at a concentration of 0.9 mM (see above and Table 2).

As in the previous model, interaction of uptake with extracellular glutamate was computed from glutamate (Glu) binding to transporters (T), with the full cycling rate k_2 reflecting the reappearance of free transporters,

$$\mathrm{Glu_0} + \mathrm{T_0} \underset{k_{-1}}{\overset{k_1}{\longleftrightarrow}} \mathrm{GluT} \xrightarrow{k_2} \mathrm{Glu_i} + \mathrm{T_0},$$

where the total number of transporters, $[T_{tot}] = [T_0] + [GluT]$, remains constant. The reaction parameters matched experimental data in Table 1: $k_1 = 10^4$ M^{-1}ms^{-1}, $k_{-1} = 0.2$ ms^{-1} (GLAST/GLT), or $k_{-1} = 0.02$ (EAAT4). The cycling rate k_2 was set at 0.1 ms^{-1}, close to the reported upper limit at 36°C (Bergles and Jahr, 1998), allowing a conservative estimate for glutamate spillover. Although the full cycle of glutamate transport is a complex process that can be represented by numerous kinetics stages (Bergles and Jahr, 1997; Otis and Jahr, 1998; Bergles and Jahr, 1998; Mennerick et al., 1999; Diamond et al., 1998; Otis and Kavanaugh, 2000; Diamond, 2001), the simplified formula above highlights its effects on the extracellular glutamate, assuming the upper limit rate of the transporter reappearance on the cell surface ($+\partial[T_o]/\partial t$; in a more complex scheme, the transporter reappearance may involve more than one kinetic step). Assuming the unchanged concentration of the ions necessary for glutamate transport (Na^+, K^+, H^+), the transport current can be estimated as k[GluT], where constant k is the rate of the reaction that is subsequent to glutamate binding, e.g., rapid translocation (Auger and Attwell, 2000). The time course of this current, therefore, will be determined by the time course of the bound glutamate level, [GluT].

RESULTS

Probabilistic pattern of perisynaptic glia

Figure 1 *A* shows a characteristic electron micrograph of the PF synapse where the neighboring glial profiles (identified from serial sections) are highlighted. In line with previous observations (Spacek, 1985; Xu-Friedman et al., 2001), glial processes often appear in the immediate vicinity of these synapses (unlike synapses in area CA1). Because of these glial sheaths, we first asked whether the extracellular space around the PF synapses differed from the homogeneous medium described earlier for the area CA1 synapses (Rusakov and Kullmann, 1998). Following the previously described methodology, we transformed electron micrographs of the PF synapses into the one-pixel binary outlines of the extracellular space profile (Fig. 1 *B*), aligned them with respect to the synaptic cleft center and then fused (averaged) the entire stack of such images. Because of the inherent rotational symmetry around the central axis perpendicular to the synaptic cleft, each profile was used along with its mirror image. In the resulting diagram (Fig. 1 *C*), the gray levels are proportional to the occurrence of the extracellular space in a plane that is roughly perpendicular to the synaptic cleft plane. The diagram reveals the synaptic apposition cleft (darker area in the middle, 0.4–0.5 μm in length) and two consistent obstacles to diffusion (paler areas adjacent to the cleft). Outside this arrangement, the extracellular space was distributed relatively homogenously, suggesting that the occurrence of glutamate escape routes is relatively even throughout the perisynaptic neuropil.

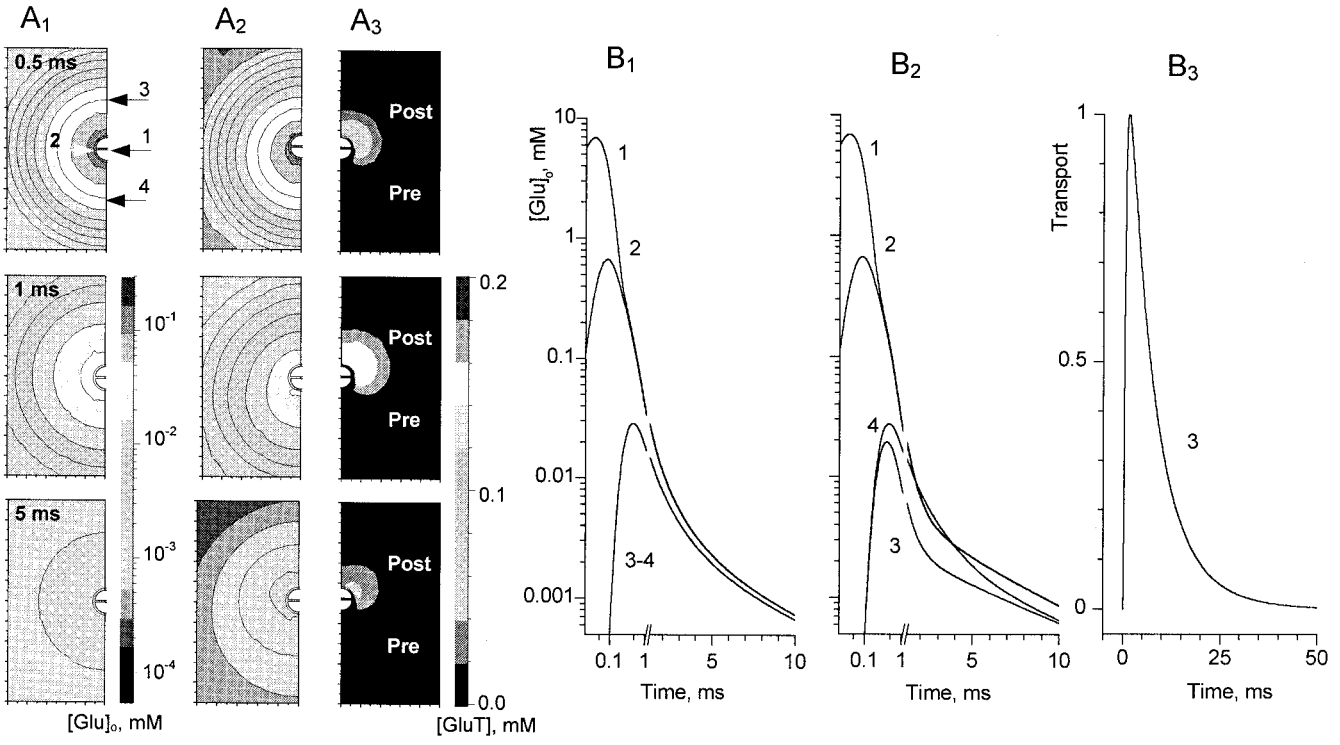

FIGURE 2 Glutamate diffusion and transport near CA1 synapses. (A_1–A_3) Concentration profile of free (A_1–A_2, logarithmic scale) and transporter bound glutamate (A_3) in the central section of a 3D synaptic environment at three time points, as indicated. Hemispheres in the center indicate the immediate pre- and postsynaptic obstacles to diffusion (see text for details). (B_1–B_3) Time course of extracellular glutamate (B_1–B_2) and of uptake current (B_3, proportional to the bound glutamate) at locations 1–4 shown by arrows in (A_1): 1, cleft center; 2, cleft edge; 3, 0.5 μm postsynaptic; 4, 0.5 μm presynaptic. (A_1, B_1) No transporters; residual glutamate binding at 10 μM. (A_{2-3}, B_{2-3}) GLAST/GLT levels match experimental data for area CA1 shown in Tables and Fig. 1. Axis ticks in panels mark 100 nm.

To estimate the probabilistic distribution of glia, we applied a similar procedure of "geometric averaging," but, in this case, all glial profiles were filled with black pixels while the rest of the image was deleted. Figure 1 *D* shows this routine applied to micrograph in Fig. 1 *A*. The transformed images were superimposed and fused, giving the average gray levels throughout the stack (80 CA1 synapses and 40 PF synapses). The resulting diagrams (Fig. 2 *E*) reflect the typical synaptic environment as seen in a 2D section perpendicular to the synaptic cleft, with gray levels proportional to the expected spatial occurrence of glia.

Although giving the characteristic occurrence of glia, these diagrams do not reveal where and how often there is a direct opposition between synaptic and glial membranes. To quantify this membrane apposition pattern, we applied another morphometrical approach. Each synaptic profile image (aligned and transformed) was divided into 16 azimuth sectors, each receiving a score of 1 or 0, depending on whether or not, respectively, the perisynaptic membrane (membrane profile that could be traced directly to the synaptic cleft) was adjacent to glia (Fig. 2 *F*). Figure 2 *G* summarizes the results throughout the micrograph stacks, showing the average score values (*gray levels*) across the sectors.

The obtained results reveal, first, a striking asymmetry in the distribution of glia. Both at CA1 and PF synapses, the occurrence of glia on the postsynaptic side is more than threefold of that on the presynaptic side. Second, the postsynaptic elements of PF synapses are likely to contact glia (~80% chance near the cleft edge and up to 95% perisynaptically), whereas such contacts at CA1 synapses are 3–4 times less frequent. We have also measured the main stereological parameters of the perisynaptic neuropil in these brain areas, which are summarized in Table 2 and indicate that near PF synapses the glia volume and cell surface fractions are ~3.4 and ~2.7 times higher than in area CA1, respectively.

What is the physiological significance of the asymmetrical distribution of glia? How different is the extent of glutamate escape, if any, in area CA1 compared to cerebellum? Do the EAAT4 transporters, which occur at the Purkinje cell dendritic spines, attenuate the glutamate transient significantly? To address these questions, we reconstructed the typical synaptic environment and simulated diffusion and transport of synaptically released glutamate in it.

Simulated glutamate transients

To dissect the effect of glial transporters, we simulated and compared glutamate diffusion in two cases. In the first case (Fig. 2, A_1 and B_1), the transporters were not available, and

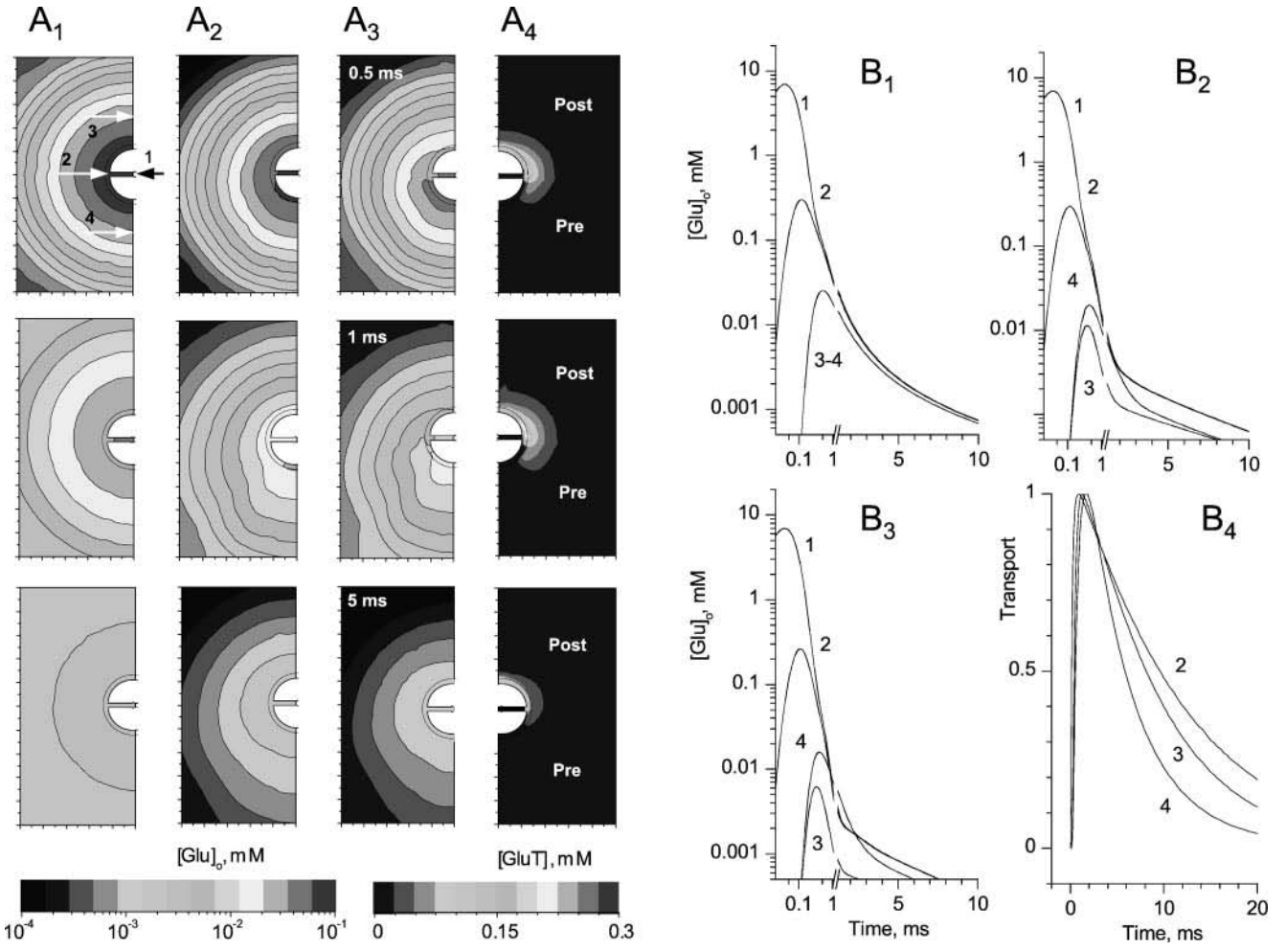

FIGURE 3 Glutamate diffusion and transport near parallel fiber synapses. (A_1–A_4) Concentration profile of free (A_1–A_3, logarithmic scale) and transporter bound glutamate (A_4). (B_1–B_4) Time course of extracellular glutamate (B_1–B_3) and of uptake current (B_4) at locations 1–4 shown by arrows in (A_1). (A_1, B_1) No transporters; residual glutamate binding at 10 μM. (A_{2-3}, B_{2-3}) GLAST/GLT levels match experimental data. (A_4, B_4) Both GLAST/GLT and EAAT4 levels match experimental data (see text). Other notations are the same as in Fig. 2.

the residual glutamate binding was set to match the estimated average level of synaptic receptors (10 μM). In the second case (Fig. 2, A_2 and B_2), the GLAST/GLT levels matched the observed experimental pattern (see Fig. 1, *E* and *G*) predicting a two- to threefold difference between the pre- and postsynaptic glutamate transients. The concentration ratio between sites 3 and 4, which are post- and presynaptic, respectively, exceeds 2.0 between 0.94 and 3.36 ms post-release, reaching the maximum of 2.69 at 1.9 ms (see Fig. 2, B_1 and B_2). Yet, free glutamate appears to remain above a 1–2-μM level within an ~0.5-μm-wide area around the synapse 5 ms post-release (Fig. 2 B_2), which is consistent with predictions of previous models (Rusakov and Kullmann, 1998; Rusakov, 2001; however, see Barbour and Hausser, 1997). Interestingly, the unbinding of glutamate from transporters appears to provide some additional perisynaptic source of free glutamate at a later stage post-release (compare Fig. 2 A_2, 1-ms and 5-ms panels; however, see Discussion). Simulations also predict that the estimated uptake current, which is proportional to the bound glutamate level, is spatially localized in the synaptic vicinity (Fig. 2, A_3 and B_3).

The effects of transporters on extracellular glutamate escape near PF synapses are illustrated in Fig. 3. The GLAST/GLT transporters reduce the extracellular glutamate transient two- to threefold on the presynaptic side and seven- to eightfold on the postsynaptic side (compare Fig. 3, A_1 and A_2; the concentration ratio between sites 3 and 4 exceeds 2.0 between 0.52 and 2.17 ms post-release, reaching the maximum of 3.14 at 1.25 ms, see Fig. 3, B_1 and B_2). The presence of EAAT4 in postsynaptic membranes results in a further two- to fourfold reduction of the postsynaptic glutamate levels, and, therefore, a further pre- versus postsynaptic asymmetry (Fig. 3, A_3 and B_3; the concentration ratio between sites 3 and 4 exceeds 3.0 between 0.46 and 2.53 ms, reaching 6.43 at 1.22 ms). The data predict

that, postsynaptically, the glutamate concentration drops below 1 μM within 1 ms post-release and that the glial uptake current in this system is also spatially localized (Fig. 3, A_4 and B_4).

DISCUSSION

We have investigated the characteristic synaptic environment of area CA1 hippocampal synapses and PF cerebellar synapses and have found that there is a strikingly higher (three- to fourfold) occurrence of glia on the post- compared to the presynaptic side of these synapses (Fig. 1). The data also show that glia occupy ~32% of the tissue volume near PF synapses and are likely to contact the postsynaptic elements directly (Fig. 1, *E* and *G*, Table 2). The average occurrence of glial membranes adjacent to these synapses in 3D could be calculated from the 2D occurrence diagram in Fig. 1 *G* by weighting the occurrence value at each sector with the spherical surface area fraction that corresponds to this sector (e.g., the polar sector corresponds to the smallest surface area on a sphere). The value calculated from this procedure is ~69%, which is in good correspondence with the value of ~67% obtained recently from 3D reconstructions of neuropil in this area (Xu-Friedman et al., 2001). In contrast, glia in area CA1 occupy only ~10% of the tissue volume and contact synapses in only ~25% cases, which is generally consistent with 3D reconstruction data from area CA1 reported earlier (Ventura and Harris, 1999). We have simulated release and diffusion of glutamate in this typical environment and found that the glial transporters alone could reduce the amplitude of glutamate transients two- to threefold (Figs. 2 and 3). At the same time, because of the asymmetric distribution of transporters, the extent of glutamate escape on the postsynaptic side is two to three times lower than on the presynaptic side. When the neuronal EAAT4 transporters on Purkinje cells are involved, this asymmetry becomes five- to sevenfold.

Could this be affected by the presence of glutamate receptors within and outside the cleft? As discussed in our previous work (Rusakov, 2001), electrophysiological recordings combined with the quantitative immunogold labeling data show that there are 15–20 AMPA receptors, and 30–40 NMDA receptors accumulated mainly within the synaptic cleft at area CA1 synapses, with the receptor density decreasing sharply outside the cleft (Takumi et al., 1999; Nusser et al., 1998; Racca et al., 2000). This implies, on the one hand, that the average density of these major ionotropic receptors in the extracellular space is two orders of magnitude lower than that of glial transporters (~10 μM versus 0.5–1.0 mM). On the other hand, even if glutamate binds to all 50–100 synaptic receptor binding sites within the cleft, this represents only 1–2% of ~5000 molecules that are released by a single vesicle. It does not exclude, however, that, at larger distances from the release site, dense patches of high-affinity glutamate receptors could have a local effect on the residual glutamate transient in the extracellular space. Clearly, the synaptic environment of each individual synapse will differ from the average geometrical approximations we use. However, similar to electrophysiological generalizations, such averaging could reveal common and significant trends in the synaptic population of interest. Furthermore, there is a sound theoretical basis to believe that the properties of individual synapses are correctly reflected in the properties of the "population average" even when the synapse-to-synapse variability in these properties is high (Uteshev et al., 2000).

In our simulations, we used the transporter kinetics parameters obtained by several groups (see Table 1). However, a recent observation of a very fast uptake current in cerebellar Purkinje cells has suggested that glutamate-transporter binding is immediately followed by a fast translocation step; it was argued that this must enhance the removal of glutamate (Auger and Attwell, 2000). To test this hypothesis, we set the glutamate-transporter binding effectively irreversible (by decreasing 100-fold the off-rate constant, k_{-1}). This resulted in a 25–35% decrease in the glutamate concentration compared with the original results (Fig. 3, A_3 and B_3), which is summarized in Fig. 4 *A*. The effect was predictably moderate because the high affinity of transporters, rather than a slow cycling rate, is believed to underlie the fast removal of glutamate immediately after release (Diamond and Jahr, 1997; Rusakov and Kullmann, 1998). However, as was pointed out in the same study (Auger and Attwell, 2000), the irreversible binding would abolish the "delayed source of glutamate," or buffering, due to unbinding (predicted by our simulations for CA1 synapses; Fig. 2 A_2). Although we adopted the upper limit value of k_2 (Bergles and Jahr, 1998), other experimental estimates suggest a lower cycling rate (~15 s^{-1}, see Table 1). Setting k_2 at this lower level increased the simulated glutamate levels by 30–50% over the 1–5-ms period (data not shown); the effect was small compared to the 5–50-fold changes caused mainly by the glutamate–transporter binding.

Our data are consistent with synaptic crosstalk in area CA1, but do they predict that glutamate spillover is negligible near PF (Fig. 3, A_3 and B_3)? There is some uncertainty about the amount of glutamate released and the value of its diffusion coefficient *D*. Figure 4, *B* and *C*, illustrate the effect of varying the number of released molecules (2500 and 7500) and the value of *D* (0.1–0.6 μm^2/ms) within the physiological range. As expected, lower vesicle contents elicit smaller glutamate transients. Retarded diffusion, however, enhances spillover (with the extreme values of *D* corresponding to a five- to sixfold difference in glutamate levels), an apparently paradoxical result addressed previously (Rusakov and Kullmann, 1998). There is also uncertainty about the baseline occupancy of transporters, which depends on the ambient glutamate level (or on the rate of glutamate leakage or release). Given the steady-state baseline conditions, the glutamate binding and uptake reaction

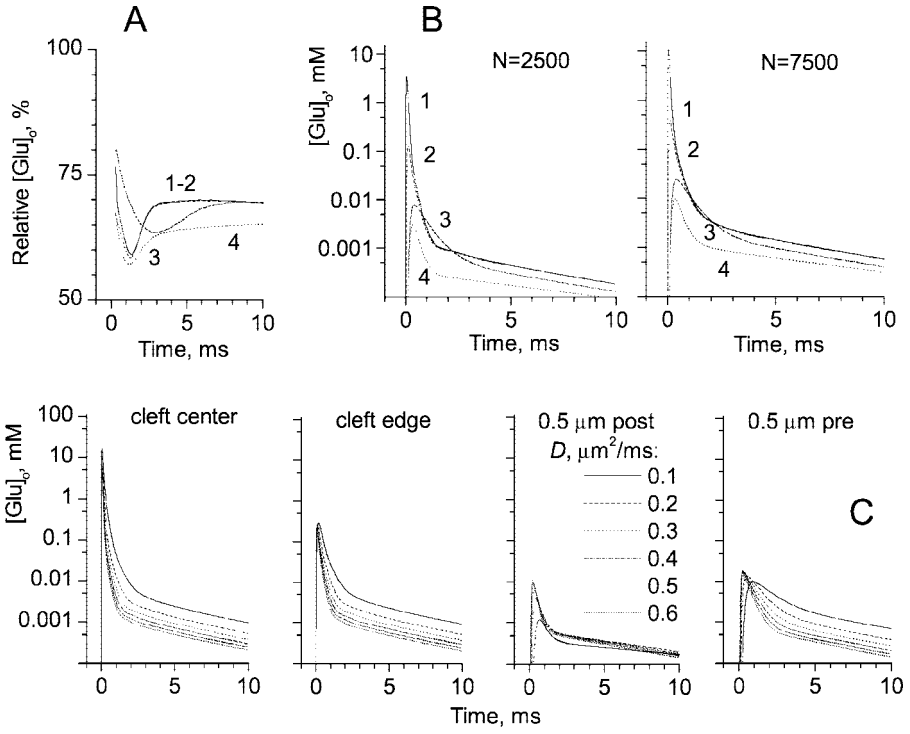

FIGURE 4 The effect of irreversible transporter binding (*A*), and varying the synaptic vesicle contents (*B*) and diffusion coefficient (*C*) on glutamate transient near PF synapses. (*A*) Extracellular glutamate time course under irreversible binding (k_{-1} is decreased 100-fold) normalized (in percent) against the baseline time course shown in Fig. 3, A_3 and B_3, at locations 1–4, as shown by arrows in Fig. 3 A_1. (*B*) Glutamate transient at four locations (1–4, see above), with 2500 or 7500 molecules released, as shown (compare with Fig. 3). (*C*) Glutamate transient at four locations (1–4, see above) for six values of diffusion coefficient *D*, as shown.

relates the total transporters level $[T_{tot}]$ to the free transporter level [T] and the resting glutamate concentration $[Glu]_o$ as follows (Rusakov and Kullmann, 1998): $[T] = (k_{-1} + k_2)[T_{tot}](k_{-1} + k_2 + k_1[Glu]_o)^{-1}$. Substituting the experimental parameters (see Tables) suggests that the ambient glutamate below 1 μM would have little effect ($<$3.2%) on the numbers of free glial transporters.

Assuming that the level of participating ions (Na^+, K^+, H^+) remains unchanged, the glutamate transporter current time course should follow the kinetics of the bound glutamate [GluT] (see above). Because this does not require any additional assumptions about the transporter cycle, we thought it would be useful to compare the computed uptake kinetics with the experimental uptake time course reported in the literature for similar synaptic circuits; this comparison could provide a plausibility test for our model using an independent set of experimental data. In the tissue, however, the uptake currents recorded in glia follow activation of multiple synapses and depend on the typical distance between active release sites and the glial membrane. Could our model predict this typical distance (single unknown parameter), within a plausible range, by matching experimental and simulated data? To test this, we systematically compared the uptake currents simulated at different (postsynaptic) distances from the release site, with the available recordings. Figure 5, *A* and *B* illustrates that the uptake current simulated at ~1.8 μm from the release site in area CA1 (Fig. 5 *A*) and at ~1.3 μm near the PF synapse (Fig. 5 *B*), provide a reasonable match with the corresponding experimental time course. The neuronal EAAT4, however, will generate the uptake current mainly within the postsynaptic spine of the activated synapse. Figure 5 *C* shows that the EAAT4 current computed by our model at the postsynaptic element of the cerebellar synapse (with no adjustable distances used) matches the fast EAAT4 current reported recently for the climbing fiber-Purkinje cell synapses (Auger and Attwell, 2000). Although our simulations use structural parameters of other synapses on Purkinje cells, the result indicates that the rapid extracellular transient of glutamate and its high-affinity binding to the transporters could explain the fast uptake currents recorded in these cells.

Our data predict a significant difference between pre- and postsynaptic glutamate concentration level following synaptic release. What might be the functional consequences of this asymmetry? In Purkinje cells, immunogold labeling has revealed that functional metabotropic glutamate receptors (mGluR1α), which respond to stimulation of PFs (Batchelor et al., 1994), tend to accumulate just outside the cleft of the PF synapses (Lujan et al., 1997); this postsynaptic locus is also enriched in EAAT4 (see above). Our results predict,

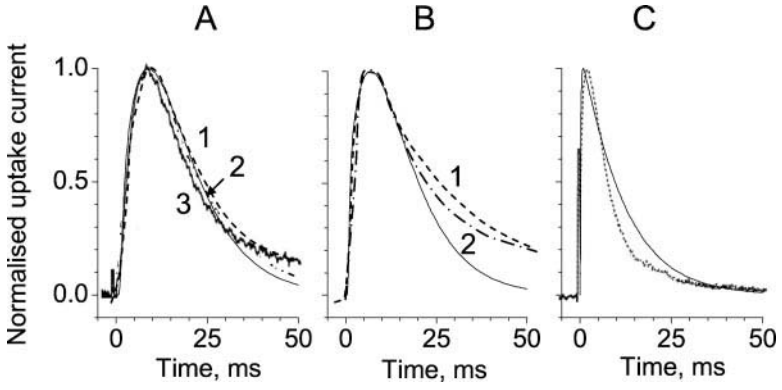

FIGURE 5 Kinetics of simulated versus recorded uptake currents. (*A*) Simulated transport current (proportional to [GluT], see Methods) near CA1 synapses at 1.8 μm form the release site (*solid smooth line*) and uptake currents recorded in hippocampal astrocytes: *1*, Bergles and Jahr, 1997; *2*, Luscher et al., 1998; *3*, Diamond et al., 1998. (*B*) Simulated transport near PF synapses at 1.3 μm from the release site (*solid line*) and uptake currents recorded in Bergmann glia: *1*, Bergles et al., 1997; *2*, Clark and Barbour, 1997. (*C*) Simulated uptake time course at the postsynaptic dendritic spine at a cerebellar synapse (*solid line*) and the uptake current recorded in Purkinje cells (*dotted line*) (Auger and Attwell; 2000). Ordinate, relative units.

therefore, that these transporters serve the purpose of reducing the activation of postsynaptic mGluRs at the PF synapses, which is immediately consistent with physiological results reported very recently (Brasnjo and Otis, 2001). Conversely, activation of presynaptic glutamate receptors with similar pharmacological properties located outside the cleft is more likely. This may favor the type of mGluR-mediated feedback signaling via glutamate spillover as has been reported at hippocampal mossy fiber synapses (Min et al., 1998; Scanziani et al., 1996; Vogt and Nicoll, 1999). In contrast, if presynaptic receptors at neighboring synapses were more exposed to the effects of glutamate spillover than were the postsynaptic receptors, it would imply that synaptic releases could exert a modulatory action on the neighboring synaptic inputs without a compatible effect on the corresponding postsynaptic targets.

The authors are indebted to Dimitri Kullmann, Niels Christian Danbolt, Jeffrey Diamond, Michael Häusser, and Arnd Roth for reading of the manuscript and valuable comments and suggestions.

This work was supported by the Medical Research Council (G120/490) and Wellcome Trust (#066031), U.K.

REFERENCES

Arriza, J. L., W. A. Fairman, J. I. Wadiche, G. H. Murdoch, M. P. Kavanaugh, and S. G. Amara. 1994. Fictional comparison of three glutamate transporter subtypes cloned from human motor cortex. *J. Neurosci.* 14:5559–5569.

Asztely, F., G. Erdemli, and D. M. Kullmann. 1997. Extrasynaptic glutamate spillover in the hippocampus: dependence on temperature and the role of active glutamate uptake. *Neuron.* 18:281–293.

Auger, C., and D. Attwell. 2000. Fast removal of synaptic glutamate by postsynaptic transporters. *Neuron.* 28:547–558.

Barbour, B., and M. Hausser. 1997. Intersynaptic diffusion of neurotransmitter. *Trends Neurosci*. 20:377–384.

Bartol, T. M., B. R. Land, E. E. Salpeter, and M. M. Salpeter. 1991. Monte Carlo simulation of miniature endplate current generation in the vertebrate neuromuscular junction. *Biophys. J.* 59:1290–1307.

Batchelor, A. M., D. J. Madge, and J. Garthwaite. 1994. Synaptic activation of metabotropic glutamate receptors in the parallel fiber–Purkinje cell pathway in rat cerebellar slices. *Neuroscience.* 63:911–915.

Bergles, D. E., J. A. Dzubay, and C. E. Jahr. 1997. Glutamate transporter currents in Bergmann glial cells follow the time course of extrasynaptic glutamate. *Proc. Natl. Acad. Sci. U.S.A.* 94:14821–14825.

Bergles, D. E., and C. E. Jahr. 1997. Synaptic activation of glutamate transporters in hippocampal astrocytes. *Neuron.* 19:1297–1308.

Bergles, D. E., and C. E. Jahr. 1998. Glial contribution to glutamate uptake at Schaffer collateral-commissural synapses in the hippocampus. *J. Neurosci.* 18:7709–7716.

Brasnjo, G., and T. S. Otis. 2001. Neuronal glutamate transporters control activation of postsynaptic metabotropic glutamate receptors and influence cerebellar long-term depression. *Neuron.* 31:607–616.

Carter, A. G., and W. G. Regehr. 2000. Prolonged synaptic currents and glutamate spillover at the parallel fiber to stellate cell synapse. *J. Neurosci.* 20:4423–4434.

Chaudhry, F. A., K. P. Lehre, M. V. Campagne, O. P. Ottersen, N. C. Danbolt, and J. Storm-Mathisen. 1995. Glutamate transporters in glial plasma membranes—highly differentiated localizations revealed by quantitative ultrastructural immunocytochemistry. *Neuron.* 15:711–720.

Clark, B. A., and B. Barbour. 1997. Currents evoked in Bergmann glial cells by parallel fibre stimulation in rat cerebellar slices. *J. Physiol.* 502:335–350.

Clements, J. D. 1996. Transmitter timecourse in the synaptic cleft: its role in central synaptic function. *Trends Neurosci.* 5:163–170.

Danbolt, N. C. 2001. Glutamate uptake. *Progr. Neurobiol.* 65:1–105.

Dehnes, Y., F. A. Chaudhry, K. Ullensvang, K. P. Lehre, J. Storm-Mathisen, and N. C. Danbolt. 1998. The glutamate transporter EAAT4 in rat cerebellar Purkinje cells: a glutamate-gated chloride channel concentrated near the synapse in parts of the dendritic membrane facing astroglia. *J. Neurosci.* 18:3606–3619.

Diamond, J. S. 2001. Neuronal glutamate transporters limit activation of NMDA receptors by neurotransmitter spillover on CA1 pyramidal cells. *J. Neurosci.* 21:8328–8338.

Diamond, J. S., D. E. Bergles, and C. E. Jahr. 1998. Glutamate release monitored with astrocyte transporter currents during LTP. *Neuron.* 21: 425–433.

Diamond, J. S., and C. E. Jahr. 1997. Transporters buffer synaptically released glutamate on a submillisecond time scale. *J. Neurosci.* 17: 4672–4687.

Fairman, W. A., R. J. Vandenberg, J. L. Arriza, M. P. Kavanaugh, and S. G. Amara. 1995. An excitatory amino acid transporter with properties of a ligand-gated chloride channel. *Nature.* 375:599–603.

Furuta, A., L. J. Martin, C. L. G. Lin, M. Dykes-Hoberg, and J. D. Rothstein. 1997. Cellular and synaptic localization of the neuronal glutamate transporters excitatory amino acid transporter 3 and 4. *Neuroscience.* 81:1031–1042.

Harvey, R. J., and R. M. A. Napper. 1988. Quantitative study of granule and Purkinje cells in the cerebellar cortex of the rat. *J. Comp. Neurol.* 274:151–157.

Kleinle, J., K. Vogt, L. Müller, W. Senn, K. Wyler, and J. Streit. 1996. Transmitter concentration profiles in the synaptic cleft: an analytical model of release and diffusion. *Biophys. J.* 71:2413–2426.

Klockner, U., T. Storck, M. Conradt, and W. Stoffel. 1994. Functional properties and substrate-specificity of the cloned L-glutamate L-aspartate transporter GLAST-1 from rat brain expressed in *Xenopus* oocytes. *J. Neurosci.* 14:5759–5765.

Kruk, P. J., H. Korn, and D. S. Faber. 1997. The effects of geometrical parameters on synaptic transmission: a Monte Carlo simulation study. *Biophys. J.* 73:2874–2890.

Lehre, K. P., and N. C. Danbolt. 1998. The number of glutamate transporter subtype molecules at glutamatergic synapses: chemical and stereological quantification in young adult rat brain. *J. Neurosci.* 18: 8751–8757.

Lehre, K. P., L. M. Levy, O. P. Ottersen, J. Storm-Mathisen, and N. C. Danbolt. 1995. Differential expression of two glial glutamate transporters in the rat brain: quantitative and immunocytochemical observations. *J. Neurosci.* 15:1835–1853.

Levy, L. M., O. Warr, and D. Attwell. 1998. Stoichiometry of the glial glutamate transporter GLT-1 expressed inducibly in a Chinese hamster ovary cell line selected for low endogenous Na^+-dependent glutamate uptake. *J. Neurosci.* 18:9620–9628.

Lujan, R., J. D. B. Roberts, R. Shigemoto, H. Ohishi, and P. Somogyi. 1997. Differential plasma membrane distribution of metabotropic glutamate receptors mGluR1 alpha, mGluR2 and mGluR5, relative to neurotransmitter release sites. *J. Chem. Neuroanat.* 13:219–241.

Luscher, C., R. C. Malenka, and R. A. Nicoll. 1998. Monitoring glutamate release during LTP with glial transporter currents. *Neuron.* 21:435–441.

Mazel, T., Z. Simonova, and E. Sykova. 1998. Diffusion heterogeneity and anisotropy in rat hippocampus. *Neuroreport.* 9:1299–1304.

Mennerick, S., W. X. Shen, W. Y. Xu, A. Benz, K. Tanaka, K. Shimamoto, K. E. Isenberg, J. E. Krause, and C. F. Zorumski. 1999. Substrate turnover by transporters curtails synaptic glutamate transients. *J. Neurosci.* 19:9242–9251.

Min, M. Y., D. A. Rusakov, and D. M. Kullmann. 1998. Activation of AMPA, kainate, and metabotropic receptors at hippocampal mossy fiber synapses: role of glutamate diffusion. *Neuron.* 21:561–570.

Nusser, Z., R. Lujan, G. Laube, J. D. B. Roberts, E. Molnar, and P. Somogyi. 1998. Cell type and pathway dependence of synaptic AMPA receptor number and variability in the hippocampus. *Neuron.* 21: 545–559.

Oliet, S. H. R., R. Piet, and D. A. Poulain. 2001. Control of glutamate clearance and synaptic efficacy by glial coverage of neurons. *Science.* 292:923–926.

Otis, T. S., and C. E. Jahr. 1998. Anion currents and predicted glutamate flux through a neuronal glutamate transporter. *J. Neurosci.* 18: 7099–7110.

Otis, T. S., and M. P. Kavanaugh. 2000. Isolation of current components and partial reaction cycles in the glial glutamate transporter EAAT2. *J. Neurosci.* 20:2749–2757.

Otis, T. S., M. P. Kavanaugh, and C. E. Jahr. 1997. Postsynaptic glutamate transport at the climbing fiber Purkinje cell synapse. *Science.* 277: 1515–1518.

Perez-Pinon, M. A., L. Tao, and C. Nicholson. 1995. Extracellular potassium, volume fraction, and tortuosity in rat hippocampal CA1, CA3, and cortical slices during ischemia. *J. Neurophysiol.* 74:565–573.

Pines, G., N. C. Danbolt, M. Bjoras, Y. M. Zhang, A. Bendahan, L. Eide, H. Koepsell, J. Storm-Mathisen, E. Seeberg, and B. I. Kanner. 1992. Cloning and expression of a rat brain L-glutamate transporter. *Nature.* 360:464–467.

Racca, C., F. A. Stephenson, P. Streit, J. D. B. Roberts, and P. Somogyi. 2000. NMDA receptor content of synapses in stratum radiatum of the hippocampal CA1 area. *J. Neurosci.* 20:2512–2522.

Rusakov, D. A. 2001. The role of perisynaptic glial sheaths in glutamate spillover and extracellular Ca^{2+} depletion. *Biophys. J.* 81:1947–1959.

Rusakov, D. A., E. Harrison, and M. G. Stewart. 1998. Synapses in hippocampus occupy only 1–2% of cell membranes and are spaced less than half-micron apart: a quantitative ultrastructural analysis with discussion of physiological implications. *Neuropharmacology.* 37: 513–521.

Rusakov, D. A., and D. M. Kullmann. 1998. Extrasynaptic glutamate diffusion in the hippocampus: ultrastructural constraints, uptake, and receptor activation. *J. Neurosci.* 18:3158–3170.

Scanziani, M., R. C. Malenka, and R. A. Nicoll. 1996. Role of intercellular interactions in heterosynaptic long-term depression. *Nature.* 380: 446–450.

Spacek, J. 1985. 3-Dimensional analysis of dendritic spines. 3. Glial sheath. *Anat. Embryol.* 171:245–252.

Stiles, J. R., D. Van Helden, T. M. Bartol, E. E. Salpeter, and M. M. Salpeter. 1996. Miniature endplate current rise times < 100 ms from improved dual recordings can be modeled with passive acetylcholine diffusion from a synaptic vesicle. *Proc. Natl. Acad. Sci. U.S.A.* 93: 5747–5752.

Takumi, Y., V. Ramirez-Leon, P. Laake, E. Rinvik, and O. P. Ottersen. 1999. Different modes of expression of AMPA and NMDA receptors in hippocampal synapses. *Nature Neurosci.* 2:618–624.

Trommershauser, J., J. Marienhagen, and A. Zippelius. 1999. Stochastic model of central synapses: slow diffusion of transmitter interacting with spatially distributed receptors and transporters. *J. Theor. Biol.* 198: 101–120.

Underwood, E. E. 1970. Quantitative Stereology. Addison-Wesley, Reading, MA.

Uteshev, V. V., J. B. Patlak, and P. S. Pennefather. 2000. Analysis and implications of equivalent uniform approximations of nonuniform unitary synaptic systems. *Biophys. J.* 79:2825–2839.

Uteshev, V. V., and P. S. Pennefather. 1996. A mathematical description of miniature postsynaptic current generation at central nervous system synapses. *Biophys. J.* 71:1256–1266.

Ventura, R., and K. M. Harris. 1999. Three-dimensional relationships between hippocampal synapses and astrocytes. *J. Neurosci.* 19: 6897–6906.

Vogt, K. E., and R. A. Nicoll. 1999. Glutamate and gamma-aminobutyric acid mediate a heterosynaptic depression at mossy fiber synapses in the hippocampus. *Proc. Natl. Acad. Sci. U.S.A.* 96:1118–1122.

Wadiche, J. I., J. L. Arriza, S. G. Amara, and M. P. Kavanaugh. 1995. Kinetics of a human glutamate transporter. *Neuron.* 14:1019–1027.

Wadiche, J. I., and M. P. Kavanaugh. 1998. Macroscopic and microscopic properties of a cloned glutamate transporter chloride channel. *J. Neurosci.* 18:7650–7661.

Wahl, L. M., C. Pouzat, and K. J. Stratford. 1996. Monte Carlo simulation of fast excitatory synaptic transmission at a hippocampal synapse. *J. Neurophysiol.* 75:597–608.

Xu-Friedman, M. A., K. M. Harris, and W. G. Regehr. 2001. Three-dimensional comparison of ultrastructural characteristics at depressing and facilitating synapses onto cerebellar Purkinje cells. *J. Neurosci.* 21:6666–6672.